

Torque bistability in the interaction between a neutron star magnetosphere and a thin accretion disc

J. T. Locsei¹ and A. Melatos¹

¹School of Physics, University of Melbourne, Parkville VIC 3010, Australia

Accepted 1988 December 15. Received 1988 December 14; in original form 1988 October 11

ABSTRACT

We present a time-dependent model of the interaction between a neutron star magnetosphere and a thin (Shakura-Sunyaev) accretion disk, where the extent of the magnetosphere is determined by balancing outward diffusion and inward advection of the stellar magnetic field at the inner edge of the disc. The nature of the equilibria available to the system is governed by the magnetic Prandtl number Pm and the ratio ξ of the corotation radius to the Alfvén radius. For $\xi \gtrsim Pm^{0.3}$, the system can occupy one of two stable states where the torques are of opposite signs. If the star is spinning up initially, in the absence of extraneous perturbations, ξ decreases until the spin-up equilibrium vanishes, the star subsequently spins down, and the torque asymptotes to zero. Vortex-in-cell simulations of the Kelvin-Helmholtz instability suggest that the transport speed across the mixing layer between the disc and magnetosphere is less than the shear speed when the layer is thin, unlike in previous models.

Key words: accretion, accretion discs – instabilities – MHD – pulsars: general – stars: neutron – X-rays: binaries

1 INTRODUCTION

A complete *time dependent* theory of mass and angular momentum transfer onto a neutron star accreting via a thin (Shakura-Sunyaev) disc needs to explain the stochastic fluctuations observed in the spin frequencies and X-ray luminosities of such systems (Bildsten et al. 1997; Baykal & Oegelman 1993), as well as regular phenomena like the negative (spin-down) torque on accreting millisecond pulsars (Galloway et al. 2002; Chakrabarty et al. 2003), quasi-periodic oscillations (QPOs) in low-mass X-ray binaries (LMXBs) (van der Klis 2001), and torque reversals (Nelson et al. 1997). Torque reversals, in which some X-ray pulsars alternate between sustained episodes of spin-up/down, present a particular challenge to theories of accretion because the transitions between spin-up/down episodes are sudden ($\sim 10\%$ of the duration of the episodes themselves).

In the standard (Ghosh & Lamb 1979a,b) picture of neutron star accretion, a thin disc is threaded by the stellar magnetic field. The torque on the star is the sum of the material torque N_{mat} carried by material falling onto the star and the torque N_B due to magnetic stresses. The material torque N_{mat} always acts to spin up the star, while the magnetic torque N_B may either spin up or spin down the star. The Ghosh-Lamb picture has been extended

in several directions to accommodate time-dependent effects. Lovelace et al. (1995) proposed that the magnetosphere could alternate between configurations with and without outflows. Li & Wickramasinghe (1998) suggested that the maximum radius where the stellar magnetic field threads the disc is constrained to small and large values, with intermediate values excluded by an unstable feedback mechanism as the magnetospheric configuration alters the disc resistivity. Torkelsson (1998) considered the interaction between a disc dynamo and the stellar magnetic field. van Kerkwijk et al. (1998) considered the possibility that the inner disc flips over, due to warping, to form a retrograde disc. Yi & Vishniac (1999) suggested that the accretion flow changes abruptly from a geometrically thin and cool Keplerian flow to a geometrically thick and hot sub-Keplerian flow, accompanied by a change from spin-up to spin-down. Spruit & Taam (1993) (ST93 hereafter) showed that the disc can become unstable, with mass accreted in bursts, based on the premise that accretion is enhanced by the Kelvin-Helmholtz instability (KHI) but inhibited when the magnetosphere rotates faster than the disc (Illarionov & Sunyaev 1975). They compared the bursts predicted by their model to the type II bursts observed from the Rapid Burster MXB 1730–355.

In this paper, we generalize the accretion model of ST93 to include torque feedback onto the star and diffusive penetration of the stellar magnetic field into the inner edge of the accretion disc, balanced by inward advection. On the

* E-mail: tlocsei@physics.unimelb.edu.au

basis of preliminary numerical simulations, we also neglect enhancement of accretion by the KHI. We present the new model in Section 2. In Section 3, we show that the disc-magnetosphere system has two stable torque states, for certain combinations of the magnetic Prandtl number P_m and the ratio ξ of the corotation radius to the Alfvén radius. If the star is initially spinning up, in the absence of extraneous perturbations, the spin-up equilibrium eventually vanishes and the star subsequently spins down. In Section 4, we show that the viscous torque in the mixing layer, omitted in the original ST93 model, is significant; when it is included, the region of parameter space for which the system has two stable torque states is reduced. In Section 5, we present the results of preliminary numerical simulations which indicate that the transport of material across the disc-magnetosphere mixing layer due to the KHI is suppressed when the mixing layer is thin. In Section 6, we discuss the implications of the generalized model for the torque reversals observed in accreting X-ray pulsars.

2 DISC-MAGNETOSPHERE COUPLING

2.1 Magnetospheric radius

We use cylindrical polar coordinates (r, ϕ, z) throughout and assume axisymmetry. The magnetospheric radius r_{m1} of the system is defined to include all material that corotates with the star (ST93). [Such a radius may not exist if the magnetic field lines are swept back all the way to the stellar surface; Ghosh et al. (1977)]. Outside r_{m1} , there is a thin, annular mixing layer $r_{m1} < r < r_{m2}$ within which the angular velocity of infalling material is brought from the Keplerian value $\Omega_K(r_{m2})$ to the stellar velocity Ω_* by magnetic torques. Once the material enters the mixing layer, it is transported on to the star on a time-scale much shorter than r_{m1}/\dot{r}_{m1} . The rate at which mass flows inward through a surface at a fixed radius r in the disc is

$$\dot{M}(r, t) = -2\pi r v_r(r, t) \Sigma(r, t), \quad (1)$$

where Σ is the surface mass density, and $v_r < 0$ is the radial drift velocity. In the steady state, \dot{M} is constant, independent of r (by continuity), and equals the accretion rate onto the star. Out of the steady state, the accretion rate onto the star is

$$\dot{M}'(t) = \dot{M}(r_{m2}, t) + 2\pi r_{m2} \dot{r}_{m2} \Sigma(r_{m2}, t), \quad (2)$$

where the second term in (2) represents mass swept up as r_{m2} changes.

We place an upper bound on the steady state value of r_{m1} by noting that the torque required to maintain corotation in the region $r < r_{m1}$ cannot exceed that provided by the magnetic shear stress, yielding (ST93)

$$r_{m1,\max} = \frac{\dot{M} \Omega_*}{\pi |S(r_{m1,\max})|}, \quad (3)$$

where $S(r)$, the magnetic stress at radius r , at the disc surface ($z = h$), is given by (Shapiro & Teukolsky 1983)

$$|S(r)| = (2\pi)^{-1} |B_z(r) B_\phi(r)|_{z=h}. \quad (4)$$

The toroidal field, generated by differential rotation, is limited to $B_\phi \lesssim B_z$, because as B_ϕ builds up, the magnetic

pressure inflates the field lines outward until they open up, destroying the magnetic link between the star and the disc (Aly 1985, 1988). Hence, we have

$$|S(r)| = \eta B^2(r) (4\pi)^{-1} \approx \eta \mu^2 r^{-6} (4\pi)^{-1}, \quad (5)$$

where $B(r)$ is the strength of the dipole field in the absence of a disc, μ is the stellar dipole moment, and $\eta \sim 1$ encapsulates our ignorance of the true (time dependent) magnetic field modified by the disc.

The system does not necessarily adjust to $r_{m1} = r_{m1,\max}$. The value of r_{m1} depends on how rapidly the magnetic field (which induces corotation) penetrates the disc by Ohmic diffusion. Let $d_B = r_{m2} - r_{m1}$ be the depth to which the magnetic field penetrates the disc beyond r_{m1} , and let Δj be the change in specific angular momentum across the mixing layer, given by

$$\Delta j = r_{m1}^2 \Omega_* - r_{m2}^2 \Omega_K(r_{m2}). \quad (6)$$

Define d_c to be the critical depth to which the field would need to penetrate in order to change the specific angular momentum of inflowing material by Δj , obtained by setting $\dot{M} \Delta j = -2\pi r_{m1}^2 d_c S(r_{m1})$. One then finds

$$d_c = \frac{\dot{M}(r_{m2}) \Omega_*}{2\pi S(r_{m1})} \left[\left(\frac{r_{m2}}{r_{m1}} \right)^2 \left(\frac{r_{m2}}{r_c} \right)^{-3/2} - 1 \right], \quad (7)$$

where the corotation radius is given by $r_c = (GM/\Omega_*^2)^{1/3}$, and our sign convention is such that a positive magnetic stress S subtracts angular momentum from the disc, as in ST93. Since the magnetic stress acts in the direction to bring material crossing the mixing layer into corotation, one has $\text{sgn}(S) = \text{sgn}(r_c - r_{m1})$.

In equilibrium, one has $d_B = d_c$. If the equilibrium is perturbed by increasing \dot{M} , d_c increases, inflowing material cannot be brought into corotation as it travels from r_{m2} to r_{m1} , and r_{m1} must decrease by an amount $\approx d_c - d_B$ on the local radial drift time $\approx |v_r(r_{m2})|/d_B$, giving

$$\dot{r}_{m1} \approx \frac{d_B - d_c}{d_B} |v_r(r_{m2})|. \quad (8)$$

Similarly, if the equilibrium is perturbed by reducing \dot{M} , d_c decreases, inflowing material is brought into corotation before travelling the full distance from r_{m2} to r_{m1} , and r_{m1} must increase by an amount $\approx d_B - d_c$ in a time $\approx |v_r(r_{m2})|/d_B$, as in (8).

2.2 Mixing layer thickness

The mixing layer thickness d_B is determined by a competition between outward diffusion and inward advection. Let v_B be the speed at which the magnetic field penetrates into the disc, as measured in a frame where $v_r = 0$. One finds $v_B \approx \nu_B/d_B$, as for any diffusive process, where ν_B is the magnetic diffusivity of the disc material. In the observers frame, where the magnetospheric radius is changing and matter flows radially inward, we have $v_B = \dot{r}_{m2} + |v_r(r_{m2})|$, and hence

$$\dot{r}_{m2} = \frac{\nu_B}{d_B} - |v_r(r_{m2})|. \quad (9)$$

It might appear, from (9), that we are erring by modelling a diffusive process as an advective one. This is not so, as is clear from the special case $\dot{r}_{m1} = 0$, $v_r(r_{m2}) = 0$, where

(9) reduces to $\dot{d}_B = \nu_B/d_B$ and hence $d_B = (2\nu_B t)^{1/2}$ for $d_B(t=0) = 0$, as expected for diffusion.

Comparing our model with ST93, we note the following. ST93 set r_{m1} to the largest value for which the corotation of material within r_{m1} can be maintained by magnetic stresses. Subsequently, they calculate the mixing layer thickness by requiring that disc material be brought into corotation by magnetic stresses before reaching r_{m1} . In our model, the mixing layer thickness is set by the advection-diffusion balance, and r_{m1} grows or shrinks depending on whether or not material can be brought into corotation as it crosses the mixing layer, as described in Section 2.1. ST93 allow for r_{m1} to decrease if the velocity shear across the mixing layer exceeds the radial drift velocity, arguing that in this case the KHI transports material across the boundary layer faster than it can be brought into corotation. In our model, material is transported across the mixing layer at the radial drift velocity. This is motivated by numerical simulations of the KHI (Section 5) showing that mass transport is inhibited in a thin mixing layer.

In both our model and ST93, magnetic stresses act only on the mixing layer, so the magnitude of the magnetic torque on the disc is smaller than in models of star-disc interactions where magnetic stresses act on the entire disc, such as Rappaport et al. (2004) (RFS04 henceforth). For an order-of-magnitude comparison, one can take the representative values $d_B = 0.01r_c$, $r_{m1} = 1.1r_c$, and integrate our assumed form of the magnetic stress $|S(r)| = \mu^2 r^{-4} (4\pi)^{-1}$ over the mixing layer, to determine the approximate magnitude of the magnetic torque on the mixing layer in our model. One can similarly calculate the magnetic torque on the disc in the RFS04 model, by integrating the assumed form of the magnetic stress in RFS04, $|S(r)| = \mu^2 r^{-4} (2\pi)^{-1} [1 - \Omega_K(r)/\Omega_*]$, over the entire disc outside r_c . We find that the magnetic torque on the mixing layer in our model is of order 0.03 times the magnetic torque on the disc in RFS04, assuming identical stellar field strengths and spin frequencies in the two models. For an alternative perspective, one can take the assumed form of the magnetic stress in RFS04 and compute the ratio of the magnetic torque integrated over the entire disc outside r_c to the torque integrated only over the region $1.1r_c < r < 1.11r_c$. We find that these torques are in the approximate ratio 1:0.008.

2.3 Surface density of the disc

The surface density of the disc outside r_{m2} evolves according to the thin disc equation

$$\frac{\partial \Sigma}{\partial t} = \frac{3}{r} \frac{\partial}{\partial r} \left[r^{1/2} \frac{\partial}{\partial r} (\nu \Sigma r^{1/2}) \right], \quad (10)$$

where ν is the kinematic viscosity. We neglect the possibility that the magnetic pressure in the mixing layer causes the disc to thicken (Wang 1987). The outer boundary condition is

$$\lim_{r \rightarrow \infty} \dot{M}(r, t) = \dot{M}_\infty, \quad (11)$$

where \dot{M}_∞ is some value set by the details of Roche lobe overflow. At the inner boundary, if $r_{m2} > r_c$, the magnetosphere presents a centrifugal barrier and one expects $\Sigma(r_{m2})$ to be larger than if $r_{m2} < r_c$ [ST93; see also

RFS04], so we choose a boundary condition of the form $\nu \Sigma(r_{m2}) \propto \exp[a(r_{m2}/r_c - 1)]$, with $a > 0$. We fix the constant of proportionality by considering steady state solutions, which have the form

$$\nu \Sigma = \frac{\dot{M}}{3\pi} \left[1 - \beta \left(\frac{r_{m2}}{r} \right)^{1/2} \right], \quad (12)$$

with $\beta < 1$ (Frank et al. 1992). If $r_{m2} = r_c$, the magnetosphere corotates with the mixing layer, so the disc structure does not depend on the location of r_{m2} (ST93) and (12) implies $\beta = 0$ and $\nu \Sigma = \dot{M}/(3\pi)$. We therefore choose the boundary condition at the inner edge to be

$$\nu \Sigma(r_{m2}) = \frac{\dot{M}(r_{m2})}{3\pi} \exp[a(r_{m2}/r_c - 1)]. \quad (13)$$

Comparison of (12) and (13) shows that

$$\beta = 1 - \exp[a(r_{m2}/r_c - 1)] \quad (14)$$

in steady state. We set $a = 1$ in this paper, except where specified otherwise. We show in Section 3 and Section 4 that our results remain qualitatively unchanged for $0 \lesssim a \lesssim 2$. The boundary condition (13) differs slightly from that in ST93, where $\nu \Sigma(r_{m2}) \propto \exp[a((r_{m2}/r_c)^{3/2} - 1)]$ and there is also a power law dependence of $\nu \Sigma(r_{m2})$ on the mass accretion rate.

The viscosity ν in ST93 is constant in time and decreases as a power law in radius. In our model, we assume that ν is constant in time and independent of radius for simplicity. Later (Section 3.5), we show that including a power law dependence of viscosity on radius leaves our results qualitatively unchanged.

2.4 Stellar spin frequency

The stellar spin frequency, Ω_* , evolves according to the equation of motion

$$I \dot{\Omega}_* = N, \quad (15)$$

where I is the star's moment of inertia and

$$N = \dot{M}' \Omega_K(r_{m2}) r_{m2}^2 + N_\nu(r_{m2}) \quad (16)$$

is the torque on the star, set equal to the rate of change of angular momentum inside the surface $r = r_{m2}$. There is no magnetic term in (16) since, by assumption, there is no magnetic stress on the disc for $r > r_{m2}$. The first term in (16) is the material torque and the second term is the viscous torque, given by

$$N_\nu = 2\pi r \nu \Sigma r^2 \frac{\partial \Omega}{\partial r}. \quad (17)$$

In the steady state, (16) reduces to

$$N = \beta \dot{M} \Omega_K(r_{m2}) r_{m2}^2. \quad (18)$$

From (14) and (18), the steady state torque on the star is positive (negative) when r_{m2} is less than (greater than) r_c . Away from the steady state, this is no longer necessarily true, since (14) and (18) hold true only in the steady state. [As matter accretes onto the star, the star's moment of inertia changes slightly, but this is a second order effect; Ghosh et al. (1977).] We show that long-term changes in Ω_* alter the equilibria of the star-disc system (Section 3.4); in contrast, ST93 held Ω_* constant.

2.5 Order-of-magnitude estimates of physical quantities

In this section, we estimate the key physical parameters in the problem for typical systems. Let $M_{1.4}$, I_{45} , P_{10} , and \dot{M}_{-9} denote the mass, moment of inertia, spin period and accretion rate of a neutron star, normalised by $M = 1.4 \text{ M}_\odot$, $I = 10^{45} \text{ g cm}^2$, $P_{\text{spin}} = 10 \text{ s}$, and $\dot{M} = 10^{-9} \text{ M}_\odot \text{ yr}^{-1}$ respectively.

The corotation radius, defined by $\Omega_* = \Omega_K(r_c)$, is given by

$$r_c = 7.78 \times 10^8 M_{1.4}^{1/3} P_{10}^{2/3} \text{ cm}. \quad (19)$$

The characteristic torque N_{char} at the corotation radius is

$$N_{\text{char}} = \dot{M} (G M r_c)^{1/2} \quad (20)$$

$$= 2.40 \times 10^{34} \dot{M}_{-9} M_{1.4}^{2/3} P_{10}^{1/3} \text{ g cm}^2 \text{ s}^{-2}. \quad (21)$$

The corresponding rate of change of the spin frequency is

$$\dot{\Omega}_{*,\text{char}}/(2\pi) = 38.2 \times 10^{-13} I_{45}^{-1} \dot{M}_{-9} M_{1.4}^{2/3} P_{10}^{1/3} \text{ Hz s}^{-1}. \quad (22)$$

Pulsars exhibiting torque reversals spin up (or down) at a comparable rate, with $|\dot{\Omega}_*/(2\pi)| = 7\text{--}60 \text{ Hz s}^{-1}$ (Nelson et al. 1997). In Section 3.1, we show that our model predicts spin up/down rates of this order of magnitude.

The kinematic viscosity in a disc is conventionally parametrized by the α parameter (Shakura & Sunyaev 1973). From the standard unmagnetised α -disc solution (Frank et al. 1992),

$$\nu = 4.0 \times 10^{12} \alpha^{4/5} \dot{M}_{-9}^{3/10} M_{1.4}^{-1/4} (r/10^9 \text{ cm}) \text{ cm}^2 \text{ s}^{-1}, \quad (23)$$

taking $r \approx r_c$ and $0.001 < \alpha < 1.0$, we conclude that ν lies in the range 10^{10} to $10^{13} \text{ cm}^2 \text{ s}^{-1}$. It is convenient to define the viscous time-scale corresponding to the length-scale r_c ,

$$\tau_\nu = 2r_c^2/(3\nu) \quad (24)$$

$$= 4.06 \times 10^4 M_{1.4}^{2/3} P_{10}^{4/3} \nu_{13}^{-1} \text{ s}, \quad (25)$$

with $\nu_{13} = \nu/(10^{13} \text{ cm}^2 \text{ s}^{-1})$. Using the above estimates for ν and r_c , we find τ_ν in the range 1 to 10^3 day; this is the time-scale for torque transitions in our model (Section 3.3). By comparison, Torkelsson (1998) found τ_ν to be typically less than 0.5 day.

If the magnetic diffusivity is due to the same turbulence that is responsible for the kinematic viscosity [e.g. the magneto-rotational instability of Balbus & Hawley (1991)], one expects the magnetic Prandtl number to satisfy $\text{Pm} = \nu_B/\nu \sim 1$. By contrast, in the literature dealing with the diffusion of magnetic fields through discs, Pm is frequently considered as a free parameter in the range $10^{-2} \lesssim \text{Pm} \lesssim 10^2$ (Reyes-Ruiz & Stepinski 1996; Lubow et al. 1994). The work in this paper is valid for $\text{Pm} \ll 1$, since for higher Pm the mixing layer is not thin (Section 3).

3 TORQUE BISTABILITY

In this section, we show that the model of the disc-magnetosphere interaction presented in Section 2 possesses two stable equilibria, with opposite signs of torque, under certain conditions. In searching for equilibria, we note that the time-scale $\Omega_*/\dot{\Omega}_* \sim 10^{13} \text{ s}$ is longer than the time-scale τ_ν for $r_{\text{m}1}$ and d_B to change. Referring to (8) and (9), we observe that the condition for equilibrium is

$$d_B = \nu_B / |v_r(r_{\text{m}2})| = d_c \quad (26)$$

First, we obtain dimensionless expressions for d_B , d_c and $r_{\text{m}1,\text{max}}$ in equilibrium. From (26), (13), (1), and the definition of the Prandtl number $\text{Pm} = \nu_B/\nu$, we find

$$d_B/r_c = \frac{2}{3} \frac{r_{\text{m}2}}{r_c} \text{Pm} \exp[a(r_{\text{m}2}/r_c - 1)]. \quad (27)$$

A thin mixing layer ($d_B \ll r_c$) therefore requires a small Prandtl number (Section 2.5). From (7) and (5), we find

$$\begin{aligned} d_c/r_c &= \xi^{7/2} \sqrt{2} (r_{\text{m}1}/r_c)^6 \text{sgn}(r_c - r_{\text{m}1}) \\ &\times \left[\left(\frac{r_{\text{m}2}}{r_{\text{m}1}} \right)^2 \left(\frac{r_{\text{m}2}}{r_c} \right)^{-3/2} - 1 \right], \end{aligned} \quad (28)$$

where

$$\xi = \eta^{-2/7} r_c/r_A \quad (29)$$

is a dimensionless parameter, and

$$r_A = \left(\frac{\mu^4}{2GMM^2} \right)^{1/7} \quad (30)$$

is the characteristic Alfvén radius for spherical accretion (Elsner & Lamb 1977). From (3), (5) and (30), we find

$$r_{\text{m}1,\text{max}}/r_c = 2^{-3/10} \xi^{-7/10}. \quad (31)$$

Anticipating that $r_{\text{m}1} \sim r_c$, we initially restrict our investigation to the regime $\xi \leq 2^{-3/10}$, $r_{\text{m}1,\text{max}} \geq r_c$, so that the constraint $r_{\text{m}1} \leq r_{\text{m}1,\text{max}}$ is satisfied.

We now find equilibria by plotting d_B/r_c and d_c/r_c against $r_{\text{m}2}/r_c$ and solving (26) graphically. Equations (26), (27) and (28) *always admit one solution* for $r_{\text{m}2} > r_c$, which we denote *A* (see Fig. 1). This is a spin-down equilibrium, since the torque is negative whenever $r_{\text{m}2} > r_c$ (Section 2.4).

3.1 Multiple equilibria

Under certain conditions, two other equilibria become available to the system. The top panel of Fig. 1 shows that for $\xi = 0.35$, $\text{Pm} = 0.01$, the curves of d_B/r_c and d_c/r_c as functions of $r_{\text{m}2}/r_c$ have only a single intersection, so the disc-magnetosphere system has only a single, spin-down, equilibrium, denoted *A*. However, setting $\xi = 0.40$, $\text{Pm} = 0.01$, as in the bottom panel of Fig. 1, one finds that the curves of d_B/r_c and d_c/r_c have three intersections, and hence the disc-magnetosphere system has three equilibria, denoted *A*, *B*, *C*. These equilibria have $r_{\text{m}2}^{(A)} = 1.08r_c$, $r_{\text{m}2}^{(B)} = 0.90r_c$, and $r_{\text{m}2}^{(C)} = 0.56r_c$, so *A* is a spin-down equilibrium while *B* and *C* are spin-up equilibria. Combining (18) and (20), one obtains

$$\dot{\Omega}_* = \beta (r_{\text{m}2}/r_c)^{1/2} \dot{\Omega}_{*,\text{char}}, \quad (32)$$

giving $\dot{\Omega}_*^{(A)} = -0.082 \dot{\Omega}_{*,\text{char}}$, $\dot{\Omega}_*^{(B)} = 0.089 \dot{\Omega}_{*,\text{char}}$, and $\dot{\Omega}_*^{(C)} = 0.27 \dot{\Omega}_{*,\text{char}}$. In Section 3.2 we show that equilibria *A* and *C* are stable to perturbations in $r_{\text{m}1}$ and $r_{\text{m}2}$, while equilibrium *B* is unstable. The system is thus *bistable*, with the two stable equilibria having opposite signs of torque.

A single equilibrium trifurcates into three equilibria when the curves of d_B/r_c and d_c/r_c in Fig. 1 are tangential at some $r_{\text{m}2} < r_c$. Solving for this condition numerically, we obtain Fig. 2, which shows the combinations of Pm and ξ for which multiple equilibria exist. For $a = 1$, the critical

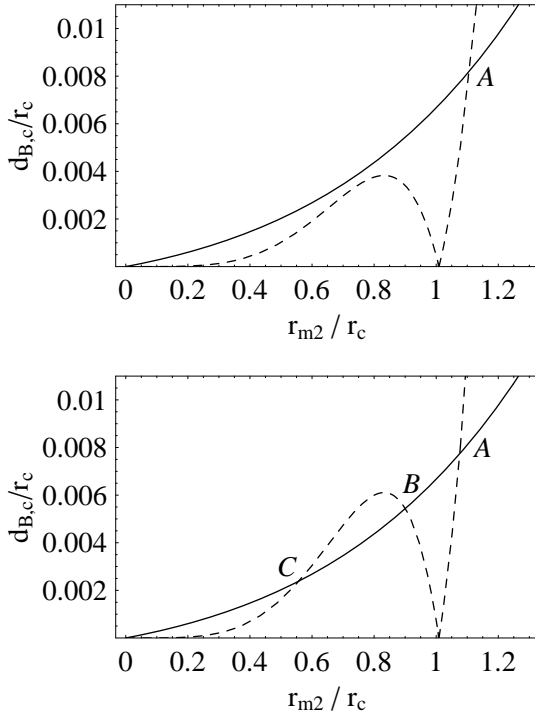


Figure 1. Equilibrium states for the disc-magnetosphere system. The top panel shows d_B/r_c (solid curve) and d_c/r_c (dashed curve) as functions of r_{m2}/r_c , for $Pm = 0.01$, $\xi = 0.35$. There is only one equilibrium, marked A , corresponding to spin down. The bottom panel shows the same information but for $Pm = 0.01$, $\xi = 0.4$. There are two stable equilibria, marked A and C , which correspond to spin-down and spin-up respectively, and one unstable spin-down equilibrium, marked B .

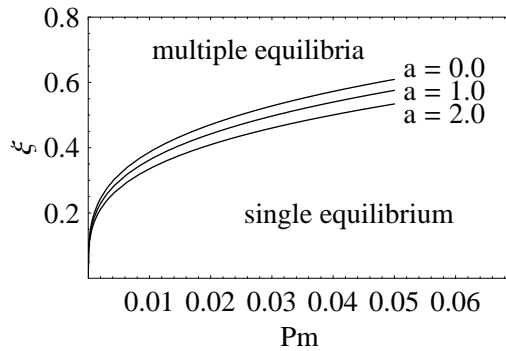


Figure 2. Combinations of Prandtl number Pm and ratio ξ of corotation radius to Alfvén radius, for which the disc-magnetosphere system has a single equilibrium and multiple equilibria. Curves for $0 \leq a \leq 2$ are plotted.

value ξ_{crit} separating the single and multiple equilibria is well approximated by

$$\xi_{\text{crit}} = 1.36 Pm^{0.287}, \quad (33)$$

with a fractional error of $< 1\%$ in the range $0 < Pm < 0.05$.

The existence of multiple equilibria can be understood as follows. One can think of d_c as measuring how ‘difficult’ it is for magnetic stresses to change the angular velocity of infalling material from $\Omega_K(r_{m2})$ to Ω_* as it crosses the mix-

ing layer. At $r_{m2} \approx r_c$, there is no velocity shear across the mixing layer, so $d_c \approx 0$. As r_{m2} is displaced from r_c , the velocity shear increases and hence d_c increases. For small enough r_{m2} , d_c decreases again because the magnetic stress is proportional to r_{m1}^{-6} , so it becomes ‘easy’ for the magnetic field to bring material crossing the mixing layer into corotation. The shape of d_c as a function of r_{m1} suggests that even if d_B was determined differently than in Section 2.2 (e.g. with a more sophisticated model of diffusion, or modified by the action of the KHI), $d_B(r_{m2})$ and $d_c(r_{m2})$ might still have multiple intersections and bistability might still occur.

3.2 Stability

Suppose that an equilibrium is perturbed by slightly increasing r_{m1} . From (8), if $d_B - d_c > 0$, r_{m1} will continue to increase, whereas if $d_B - d_c < 0$, r_{m1} will tend back to the equilibrium value. This suggests that those equilibria for which $d_B - d_c$ is a decreasing (increasing) function of r_{m2} are stable (unstable). Thus we expect equilibria A and C to be stable, and equilibrium B to be unstable.

Elaborating on the above argument, we calculate the evolution of a perturbation about each equilibrium. As a (rough) first approximation to the equations of motion, we assume that changes in the surface density profile of the disc occur rapidly compared to changes in r_{m1} , so that $\Sigma(r, t)$ can be regarded as passing through a succession of equilibrium states given by (12). In reality, r_{m1} and Σ change on similar time-scales; Σ adjusts over a length-scale r_{m1} in a time $\sim r_{m1}^2/\nu$ (Frank et al. 1992, p.70), while the radial drift velocity in a thin disc

$$v_r = \frac{-3}{\Sigma r^{1/2}} \frac{\partial}{\partial r} (\nu \Sigma r^{1/2}), \quad (34)$$

together with (8), implies $r_{m1}/\dot{r}_{m1} \sim r_{m1}^2/\nu$. None the less, in our approximation, we find the following evolution equations

$$\tau_\nu \frac{d}{dt} \left(\frac{r_{m1}}{r_c} \right) = \frac{d_B - d_c}{d_B} \frac{r_c}{r_{m2}} \exp[a(1 - r_{m2}/r_c)] \quad (35)$$

$$\equiv f_1,$$

$$\tau_\nu \frac{d}{dt} \left(\frac{r_{m2}}{r_c} \right) = \frac{2}{3} Pm \frac{r_c}{d_B} - \frac{r_c}{r_{m2}} \exp[a(1 - r_{m2}/r_c)] \quad (36)$$

$$\equiv f_2,$$

where the instantaneous value of d_c is given by (28), τ_ν is given by (24), and $d_B = r_{m2} - r_{m1}$.

Linearising about an equilibrium $[r_{m1}^{(\text{eq})}, r_{m2}^{(\text{eq})}]$, we write the equations of motion in the form $\tau_\nu \dot{x}_i = A_{ij} x_j$, with $\mathbf{x} = [(r_{m1} - r_{m1}^{(\text{eq})})/r_c, (r_{m2} - r_{m2}^{(\text{eq})})/r_c]$ and $A_{ij} = \partial f_i / \partial x_j$. The eigenvalues of A_{ij} give the growth rate of perturbations. Obtaining analytic expressions for the growth rates is not tractable, so we calculate them numerically. For equilibria A , B and C of Fig. 1, we find that the dominant modes of a perturbation have growth rates of -7.1, 3.8, and -4.7 respectively, in units of τ_ν^{-1} , indicating that A and C are stable, while B is unstable.

We emphasise that the above analysis provides an indication of stability only, since it is based on the assumption that changes in the surface density profile of the disc are

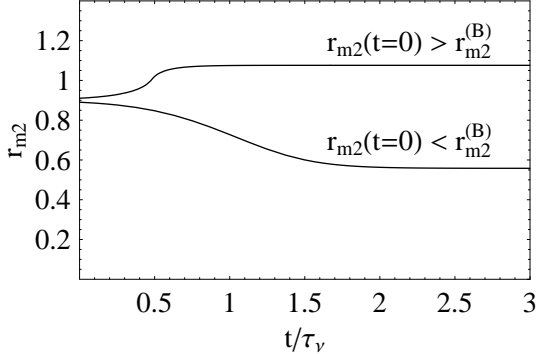


Figure 3. Transitions between equilibria, for the system in the bottom panel of Fig. 1. If the system starts with r_{m2} larger (smaller) than $r_{m2}^{(B)}$, it switches to equilibrium A (C).

rapid compared to changes in the position of the magnetosphere. To prove stability rigorously, one must solve the disc PDEs subject to our chosen boundary conditions (e.g. ST93). However, this lies beyond the scope of this paper, especially in view of the uncertainties surrounding the boundary conditions themselves (e.g. the true, time dependent nature of the magnetic field in the vicinity of the mixing layer is unknown).

3.3 Externally driven evolution

How does the bistable system in Section 3.1 switch from one equilibrium to another? One possibility is that an extraneous perturbation, such as a change in \dot{M}_∞ , pushes the system from A , through B (which is unstable), to C , in Fig. 1. To explore this possibility, we integrate the equations of motion (35) and (36), starting near the unstable equilibrium B . Typical results are shown in Fig. 3. One finds that the system tends to either of the stable equilibria, depending on the initial conditions. In each case, we set the initial value of d_B to the value corresponding to equilibrium B , but we set the initial value of r_{m2} to be slightly larger (smaller) than $r_{m2}^{(B)}$, whereupon the system tends to A (C). In each case, the transition between equilibria occurs on a time-scale $\sim \tau_\nu$.

3.4 Long-term evolution due to torque feedback

The system can also switch from one equilibrium to another as Ω_* changes secularly in response to the disc torque. To explore this possibility, let us assume that the system is initially in a state of spin-up (equilibrium C). From (29), $\xi \propto r_c \propto \Omega_*^{-2/3}$, so as the star spins up, ξ decreases, the system moves from the upper to the lower region of parameter space in Fig. 2, and equilibria B and C vanish. The system then occupies the remaining equilibrium, A , and spins down. From (31), $r_{m1,\max}/r_c \propto \xi^{-7/10} \propto \Omega_*^{7/15}$, so as the star spins down, $r_{m1,\max}/r_c$ decreases, until the state $r_{m1} = r_{m1,\max}$ is reached. Ultimately, $r_{m1,\max}$ approaches r_c , the torque tends to zero, and the system stops spinning down.

Due to the dependences of ξ and $r_{m1,\max}/r_c$ on Ω_* , Ω_* undergoes fractional changes of order unity in this evolutionary scenario. For example, suppose $Pm = 1$, $\xi = 0.4$, and initially $\Omega_* = 1$ in arbitrary units. Then the star spins up

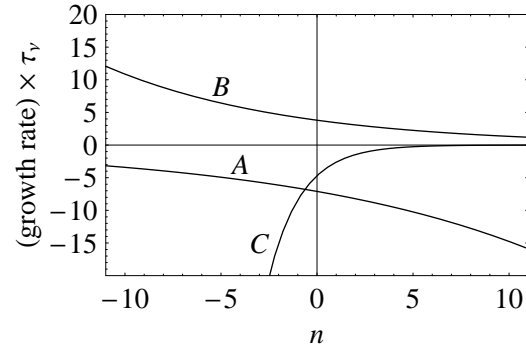


Figure 4. Growth rates of perturbations about equilibria A , B and C , for the system in the bottom panel of Fig. 1, as functions of the power law n governing the disc viscosity. As n varies, the growth rates change in magnitude but not in sign.

to $\Omega_* = 1.16$, and subsequently spins down, with $\Omega_* \rightarrow 0.40$ as $t \rightarrow \infty$.

3.5 Radial viscosity gradient

Thus far we have assumed that the viscosity is constant in time and independent of radius, whereas in ST93 ν was allowed to vary as a power law in radius:

$$\nu(r) = \nu(r_c) (r/r_c)^n. \quad (37)$$

Adopting this prescription in our model, we find that the locations of the equilibria presented in Section 3.1 are unchanged, provided that we take Pm to be uniform (for simplicity). This is because the derivations of (27) and (28) do not rely upon the assumption of uniform ν . With regard to the stability analysis in Section 3.2, one finds that the evolution equations (35) and (36) are each modified by a factor of $(r_{m2}/r_c)^n$ on the right hand sides, and the ν appearing in (24) is given by $\nu(r_c)$. Numerical evaluation of the dominant linear growth rate (maximum eigenvalue of A_{ij}), for a range of n , reveals that the growth rate changes in magnitude but not in sign (Figure 4), so the stability of each equilibrium is qualitatively unchanged from the case of uniform viscosity.

More realistically, one might expect the viscosity ν to vary as a function of the disc temperature and density, and therefore Pm may not be uniform. The detailed study of this scenario is beyond the scope of this paper.

3.6 Wind torque

For the low magnetic Prandtl numbers adopted in this study ($Pm \approx 10^{-2}$), significant bending of the magnetic field takes place, which might lead to the formation of a centrifugal wind (e.g. Lubow et al. 1994; Reyes-Ruiz & Stepinski 1996), accompanied by a magnetic torque that removes angular momentum from the disc.

We can investigate the effect of the wind torque on our calculations with a toy model, in which we assume that a fraction δ of the field lines threading the mixing layer are open and form a wind, and the magnetic stresses associated with these field lines remove angular momentum from the mixing layer (wind torque). The remaining fraction $(1-\delta)$ of field lines threading the mixing layer are closed (connected

to the star) and can either add or subtract angular momentum from the mixing layer, as in Section 2.1, depending on the relative velocities of the star and disc. For simplicity, we assume that the toroidal field associated with the open field lines at the disc surface is equal in magnitude to the toroidal field associated with the closed field lines, though its direction may be different, giving $|S_{\text{wind}}| \approx \eta\mu^2 r^{-6}(4\pi)^{-1}$.

In this crude picture, the wind torque modifies the equation for d_c , since d_c is calculated by equating the magnetic torque on the mixing layer to the rate of change of angular momentum of material crossing the mixing layer. In the case $r_{\text{m1}} < r_c$, both the open and closed field lines subtract angular momentum from the mixing layer, and one finds that equation (28) for d_c is unchanged. In the case $r_{\text{m1}} > r_c$, the closed field lines add angular momentum to the mixing layer while the open field lines subtract angular momentum from the mixing layer, and one finds that (28) is modified by a factor of $1/(1-2\delta)$ on the right hand side. For $0 < \delta < 1/2$, this has the effect of elevating the section of the curve of d_c to the right of r_c in Figure 1, so that equilibrium *A* occurs closer to corotation. For $\delta > 1/2$, one has $d_c < 0$ for $r_{\text{m1}} > r_c$, so equilibrium *A* vanishes, and it is possible that there are no solutions for equilibria; the toy model breaks down.

In our calculations, with or without the toy model for the wind, we have neglected magnetic torques on the disc outside the mixing layer. It is possible that there is a wind and an associated wind torque in this region. The wind torque might even dominate the viscous torque (see for example Pelletier 1992), and the omission of this torque is a limitation of our model.

4 VISCOSUS TORQUE AT THE MIXING LAYER

The net torque exerted on the mixing layer induces the corotation of inflowing material and hence governs the evolution of the magnetosphere. It is the sum of magnetic and viscous components. The magnetic component results from the magnetic stresses integrated over the top and bottom surfaces of the mixing layer (at $|z| = h$), while the viscous component results from the mechanical shear stress integrated over the surface $r = r_{\text{m2}}$. In this section, we show that the viscous torque, neglected by ST93, is actually $\sim r_{\text{m2}}/d_B$ times larger than the magnetic torque. When the viscous torque is included in our model, only one stable equilibrium is available to the disc-magnetosphere system under a wider range of conditions than otherwise, although this depends sensitively on the velocity profile near r_{m2} .

4.1 Ratio of viscous and magnetic torques

Material within r_{m1} corotates with the star, so the viscous stress vanishes at the inner edge of the mixing layer. By assumption, the angular velocity profile of the disc is approximately Keplerian beyond r_{m2} . The viscous torque N_ν acting on the mixing layer is therefore

$$N_\nu = 2\pi r_{\text{m2}} \nu \Sigma r_{\text{m2}}^2 \left(\frac{\partial \Omega}{\partial r} \right)_{r=r_{\text{m2}}} \quad (38)$$

$$= -3\pi \nu \Sigma(r_{\text{m2}}) \Omega_K(r_{\text{m2}}) r_{\text{m2}}^2. \quad (39)$$

The negative sign indicates that the viscous torque subtracts angular momentum from material in the mixing layer. In the steady state, at r_{m2} , the surface density is given by $\nu \Sigma(r_{\text{m2}}) = \dot{M}(1-\beta)/(3\pi)$, implying

$$|N_\nu| = \dot{M} \Omega_K(r_{\text{m2}}) r_{\text{m2}}^2 |1 - \beta|. \quad (40)$$

Note that, for fixed \dot{M} , $|N_\nu|$ does not tend to zero in the limit $\nu \rightarrow 0$, since (40) is independent of ν . In this limit, from (34), $v_r \propto \nu$ tends to zero, and $\Sigma \propto \dot{M}/v_r \propto \nu^{-1}$ grows without bound, in such a way that $N_\nu \propto \nu \Sigma$ remains fixed.

The magnetic torque N_B on the mixing layer is

$$N_B = -2\pi r_{\text{m1}} d_B S(r_{\text{m1}}) r_{\text{m1}}. \quad (41)$$

From (3), with $r_{\text{m1}} \approx r_{\text{m1,max}}$ for order-of-magnitude purposes, we obtain $\dot{M} \Omega_* \approx \pi r_{\text{m1}} |S(r_{\text{m1}})|$, implying

$$|N_B| \approx 2r_{\text{m1}} d_B \dot{M} \Omega_*. \quad (42)$$

Dividing (40) by (42), we find

$$\begin{aligned} \left| \frac{N_\nu}{N_B} \right| &\approx \frac{1}{2} \frac{\Omega_K(r_{\text{m2}})}{\Omega_*} \frac{r_{\text{m2}}^2}{r_{\text{m1}} d_B} |1 - \beta| \\ &\approx \frac{r_{\text{m2}}}{2d_B} |1 - \beta|, \end{aligned} \quad (43)$$

where we have used $\Omega_K(r_{\text{m2}}) \approx \Omega_*$ (close to corotation) and $r_{\text{m1}} \approx r_{\text{m2}}$ (thin mixing layer). The expression (43) shows that the viscous torque is much greater than the magnetic torque for $d_B \ll r_{\text{m2}}$. Neglecting the viscous torque is not permissible, except for β close to unity.

4.2 Equilibrium states

In this section, we examine the modified equilibria of the disc-magnetosphere system after taking into account the viscous torque (38). Following a similar analysis to that presented in Section 3.1, one finds that equation (27) for d_B/r_c is still valid, but (28) needs to be modified as follows:

$$\begin{aligned} d_c/r_c &= \xi^{7/2} \sqrt{2} (r_{\text{m1}}/r_c)^6 \text{sgn}(r_c - r_{\text{m1}}) \\ &\times \left[\beta \left(\frac{r_{\text{m2}}}{r_{\text{m1}}} \right)^2 \left(\frac{r_{\text{m2}}}{r_c} \right)^{-3/2} - 1 \right], \end{aligned} \quad (44)$$

with β given by (14).

Examples of graphical solutions for equilibria, with the viscous torque included, are shown in Fig. 5. The top panel uses the same values of dimensionless parameters ($P_m = 0.01$, $\xi = 0.4$) as the bottom panel of Fig. 1, but clearly the shape of d_c as a function of r_{m2} is very different, and there is only one equilibrium. The bottom panel, with $P_m = 0.001$, $\xi = 0.4$, shows a system with three equilibria; *A* and *C* are stable, with zero and spin-up torque respectively, while equilibrium *B* is unstable. In both panels, the discontinuity in d_c arises because the magnetic torque changes sign at $r_{\text{m2}} = r_c$, while the viscous torque does not; in reality, the change in the magnetic torque occurs gradually over the domain $r_c - d_B < r_{\text{m2}} < r_c + d_B$. Fig. 6 shows the regions in P_m - ξ parameter space for which there are multiple equilibria. Note that, for a given ξ , the range of P_m giving rise to multiple equilibria is smaller compared to the case where the viscous torque is neglected (Fig. 2).

The viscous torque on the mixing layer depends on

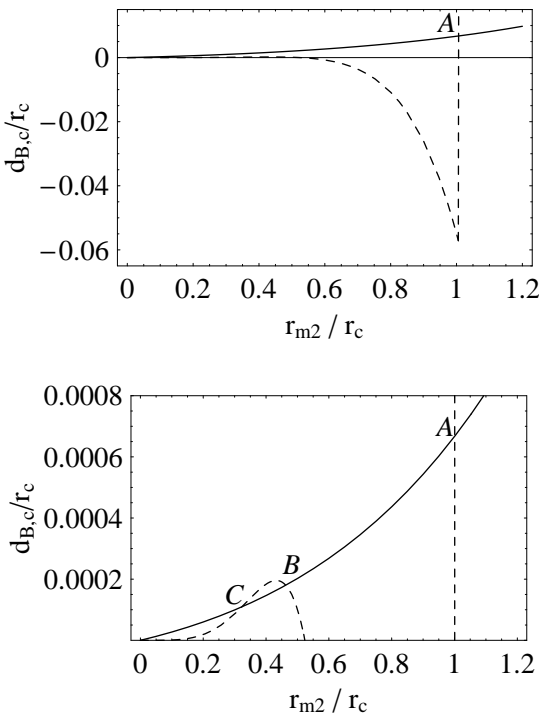


Figure 5. Equilibrium states for the disc-magnetosphere system including the viscous torque at the mixing layer. The top panel shows d_B/r_c (solid curve) and d_c/r_c (dashed curve) as functions of r_{m2}/r_c , for $Pm = 0.01$, $\xi = 0.4$. There is only one equilibrium, marked A , with zero net torque. The bottom panel shows the same information but for $Pm = 0.001$, $\xi = 0.4$. There are two stable equilibria, marked A and C , corresponding to zero torque and spin-up respectively, and one unstable, spin-up equilibrium, marked B .

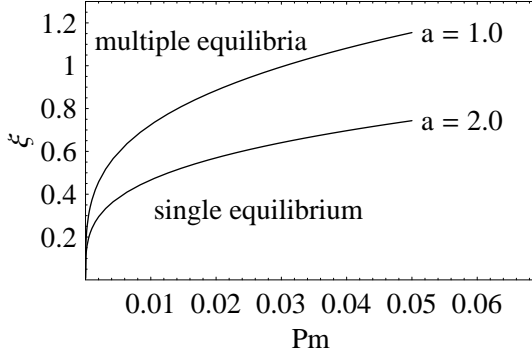


Figure 6. Regions in $Pm-\xi$ parameter space for which the system has a single equilibrium or multiple equilibria, with the viscous torque included.

$\partial\Omega/\partial r$ at r_{m2} through (38). The derivation of (44) assumes that the disc velocity profile is Keplerian beyond r_{m2} , so that the viscous torque is given by (39). This assumption is questionable, because viscous stresses may result in a nonkeplerian velocity profile for a short distance beyond r_{m2} . Fig. 7 sketches two hypothetical velocity profiles in the vicinity of the mixing layer. In one case, the velocity profile is Keplerian outside r_{m2} , and the viscous torque on the mixing layer is negative, while in the other case the velocity profile

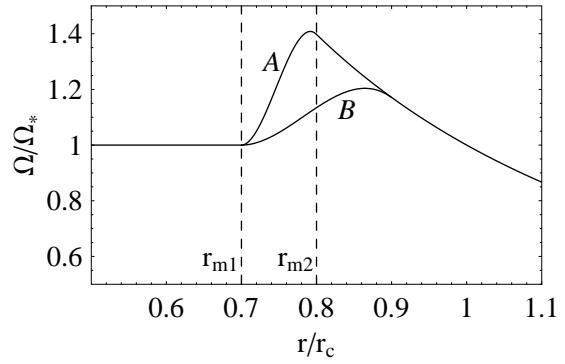


Figure 7. Schematic diagram of possible angular velocity profiles near the mixing layer (not to scale). Profile A is Keplerian beyond r_{m2} , and corresponds to a $-ve$ torque on the boundary layer ($\partial\Omega/\partial r < 0$ at r_{m2}). Profile B is non-Keplerian for a short distance beyond r_{m2} , and corresponds to a $+ve$ torque ($\partial\Omega/\partial r > 0$ at r_{m2}).

is non-Keplerian for a short distance beyond r_{m2} , and the viscous torque on the mixing layer is positive. Consequently, the system is very sensitive to the velocity profile near the mixing layer. ST93 did not address this issue, because the viscous torque on the mixing layer was neglected in their model. In the special case $\partial\Omega/\partial r = 0$ at $r = r_{m2}$, the viscous torque on the mixing layer vanishes, and the analysis in Section 3 and ST93 is valid.

5 TURBULENCE IN THE MIXING LAYER

The interaction between the accretion disc and the stellar magnetic field at the disc-magnetosphere boundary is not well understood. The boundary is subject to magnetohydrodynamic (MHD) instabilities, e.g. the magnetic interchange instability (MII) and the Kelvin-Helmholtz instability (KHI), which control the turbulent transport of material through the mixing layer, into the magnetosphere, and onto the star (Ghosh & Lamb 1978, 1979a,b; Scharlemann 1978; Spruit & Taam 1993). Such instabilities may also explain the quasi-periodic oscillations in X-ray sources (Baan 1979; Li & Narayan 2004).

In this section, we assess the validity of the claim that the KHI transports material across the mixing layer with a speed (ST93)

$$v_{KH} = r_{m1} |\Omega_K(r_{m1}) - \Omega_*|. \quad (45)$$

To this end, we wrote a vortex-in-cell (VIC) code to perform two dimensional (2D), inviscid, incompressible, hydrodynamic simulations of the KHI (with $B = 0$ and effective gravity $g_{eff} = 0$) in an elongated domain, representing a thin mixing layer (ST93). We emphasise that the simulations give some insight into the behaviour of the KHI but they do not faithfully simulate the global physics of the mixing layer. Ideally, in a full treatment, one would perform simulations in an unbounded domain and see how thick the mixing layer grows of its own accord, rather than enforcing a thin layer and testing what sort of flow is consistent with this assumption, as we do here.

5.1 Vortex-in-cell code

The VIC algorithm (Liu & Doorma 2000) discretises the vorticity field $\omega = \nabla \times \mathbf{v}$ into point vortices, or *vortons*. The vortons are tracked as particles, while the velocity field $\mathbf{v} = \nabla \times \mathbf{A}$ is obtained by solving Poisson's equation,

$$\nabla^2 \mathbf{A} = -\omega, \quad (46)$$

on a grid, where \mathbf{A} is the vector potential for the velocity field. Vortons are advected by the velocity field; in turn, one can reconstruct the velocity field from the vorton distribution.

Our simulations are performed in a 2D box of dimensions $0 < x < W = 1$, $-L/2 < y < L/2$. The velocity field is tracked on a regular cartesian grid (x, y) tiled by $n_x \times n_y$ cells. The domain is periodic in one direction,

$$\mathbf{v}(x = 0, y, t) = \mathbf{v}(x = 1, y, t), \quad (47)$$

consistent with the cylindrical geometry of the annular mixing layer. In the other direction, representing the inner and outer edges of the annulus, we set

$$v_y(x, -L/2, t) = v_y(x, L/2, t) = 0, \quad (48)$$

$$\omega(x, -L/2, t) = \omega(x, L/2, t) = 0. \quad (49)$$

To be absolutely consistent with ST93, one would prefer to specify v_x at $|y| = L/2$. Doing so, however, requires the creation of new vortons at these boundaries, a feature that is hard to implement in our code. Initially, the fluids in the inner and outer halves of the annulus are approximately counter-streaming, with $\mathbf{v}(x, y, 0) = 0.5\hat{x}$ for $y < 0$ and $\mathbf{v}(x, y, 0) = -0.5\hat{x}$ for $y > 0$. Thus, one unit of time in our simulations is equal to the length of the simulation domain divided by the shear speed; physically, this is approximately the spin period of the neutron star. To provide an initial perturbation from which the KHI can grow, each vorton is given a random initial y coordinate in the range $-0.005 < y < 0.005$, as in the top panel of Fig. 8.

5.2 Transport speed

The simulations track the root-mean-square and the maximum of the y component of velocity, $v_{y,\text{rms}}$ and $v_{y,\text{max}}$, from which we can estimate the average and maximum rates at which material is transported across the mixing layer. We performed simulations for $L = 1, 1/2, 1/4, 1/8, 1/16, 1/32$, with $n_y = 64$, $n_x = 64/L$, and 5×10^3 vortons. Fig. 8 shows that the first vortical structures form on the smallest scales λ , consistent with the linear KHI growth rate $\gamma_{\text{KHI}} \propto \lambda^{-1}$. These structures merge hierarchically until a single vortex occupies the simulation domain; energy cascades from small to large scales in 2D (Batchelor 1953). The top panel of Fig. 9 shows that $v_{y,\text{max}}$ rises initially, then decays within ~ 20 crossing times, asymptoting to a value that depends upon W/L . The top panel of Fig. 10 shows that higher aspect ratios W/L give a lower saturated value of $v_{y,\text{max}}$. The behaviour of $v_{y,\text{rms}}$ as a function of W/L is similar to $v_{y,\text{max}}$ with $v_{y,\text{rms}} \approx 0.2v_{y,\text{max}}$ (bottom panels of Fig. 9 and Fig. 10).

Our results imply that when the KHI is confined to an elongated domain, the maximum transport speed across the mixing layer is significantly less than the velocity shear.

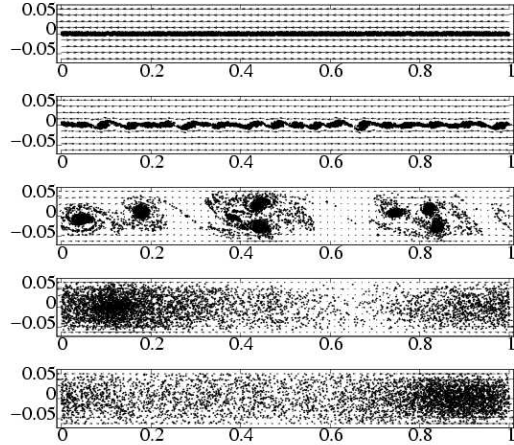


Figure 8. KHI instability in a domain of dimensions $W = 1.0$, $L = 1/8$, at times $t = 0, 0.125, 1, 10, 100$ (top to bottom). Diamonds represent vortons, and arrows show the velocity field.

However, these results must be interpreted with caution. Our simulations are 2D; they neglect the Coriolis force, gravity, magnetic fields and compressibility; and the vorticity vanishes artificially at the boundaries. One would expect the inclusion of three-dimensionality, magnetic fields and compressibility to decrease $v_{y,\text{max}}$ further, since energy cascades from large to small scales in 3D (Batchelor 1953), compressibility tends to suppress the KHI (Wang & Robertson 1984), and magnetic fields tend to disrupt large eddies (Malagoli et al. 1996). In contrast, it is hard to predict the effect of different boundary conditions, the Coriolis force, and gravity ($g_{\text{eff}} \neq 0$).

6 DISCUSSION AND CONCLUSIONS

In this paper, we present a generalized model of the disc-magnetosphere interaction, which incorporates diffusion of the stellar magnetic field into the disc. We show that, for $\xi \gtrsim \text{Pm}^{0.3}$, the system possesses two stable equilibria, corresponding to spin-up and spin-down. (Our calculations indicate rather than prove stability, since they are based on the assumption that changes in the surface density profile of the disc are rapid compared to changes in the position of the magnetosphere). We suggest that transitions between stable equilibria can be induced, on the viscous time-scale τ_{ν} , by changes in the mass accretion rate at the outer edge of the disc (extraneous) or changes in the spin frequency of the star (torque feedback). We also show that the viscous torque N_{ν} is generally much larger than the magnetic torque N_B ; when it is included, the dynamics of the disc-magnetosphere system are very sensitive to the velocity profile at r_{m2} , but typically there are fewer combinations of Pm and ξ for which the system is bistable. Preliminary numerical simulations of the KHI indicate that the transport speed across the mixing layer between the disc and magnetosphere is less than the shear speed when the layer is thin. In our model, material is transported across the mixing layer at the radial drift velocity.

Given the presence of two stable equilibria in our model,

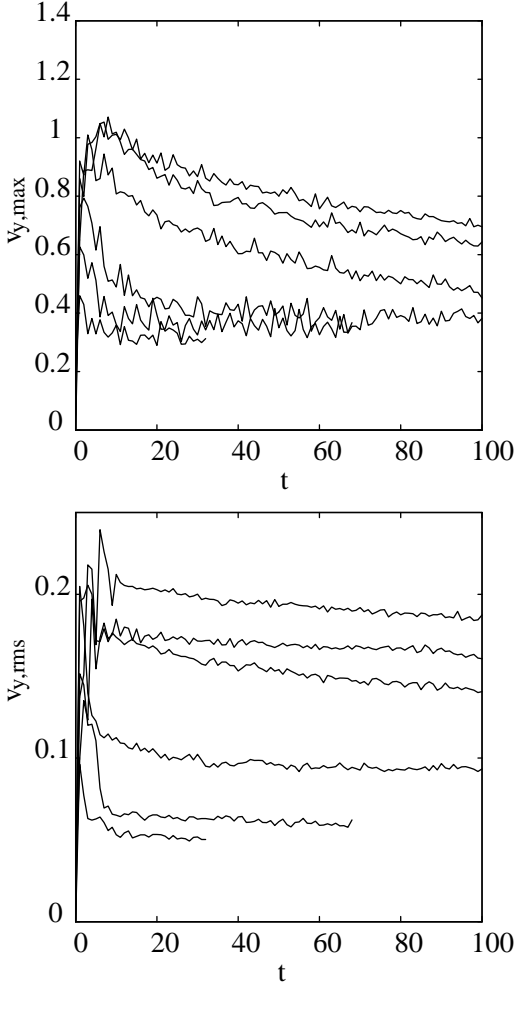


Figure 9. Maximum transport speed $v_{y,\max}$ (top panel) and root-mean-square transport speed $v_{y,\text{rms}}$ (bottom panel) due to the KHI across an elongated domain, versus time. One unit of time is approximately one stellar spin period. In each panel, curves are plotted for $W/L = 1, 2, 4, 8, 16, 32$ (top to bottom).

it is interesting to ask whether we can draw any parallels with the phenomenon of torque reversals (Nelson et al. 1997). The X-ray pulsars GX 1+4, 4U-1626-67, Cen X-3 and OAO 1657-415 have all been observed to alternate between episodes of spin-up and spin-down, such that the time-scale for transitions between episodes (days) is much shorter than the the duration of individual torque episodes (weeks or years). A successful model for torque reversals should explain the observed properties: (i) Transitions never occur between torques of the same sign (but different magnitudes). (ii) The torque ranges from $0.2N_{\text{char}}$ for 4U-1626-67 to $2.3N_{\text{char}}$ for Cen X-3, assuming $\dot{M} = 10^{-9} M_{\odot} \text{ yr}^{-1}$. (iii) The transition time-scale is much shorter than the time-scale for a sustained torque episode. (iv) The torque and luminosity are anti-correlated in the spin-down of GX 1+4. Evaluating our model against these criteria, we see the following: (i) The two stable equilibria have opposite signs of torque,

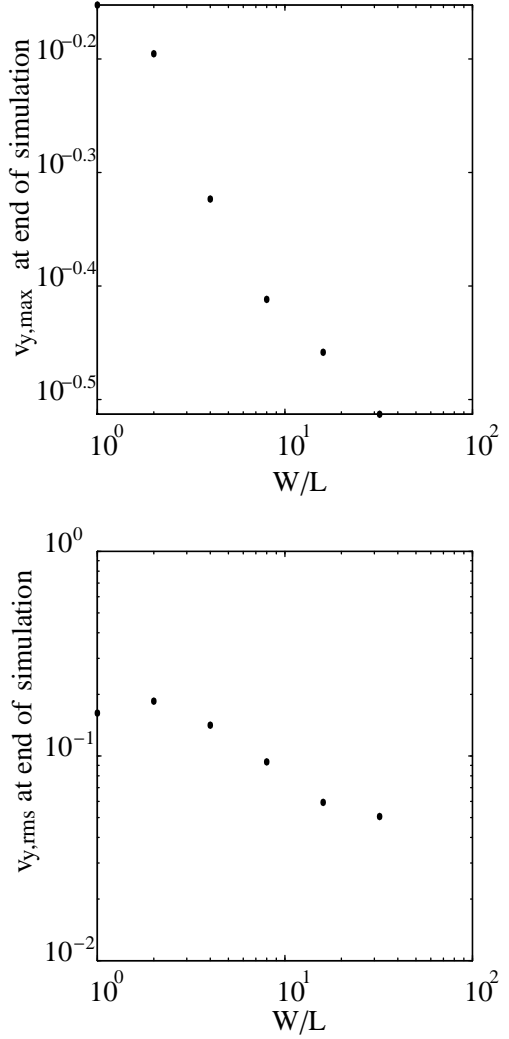


Figure 10. The mean of $v_{y,\max}$ (top panel) and $v_{y,\text{rms}}$ (bottom panel) over the last 5 time units of each simulation, as a function of W/L . One unit of time is approximately one stellar spin period.

so there are never transitions between torques of the same sign. (ii) The magnitude of the torque is $\sim 0.1N_{\text{char}}$. (iii) Transitions between equilibria occur over ~ 1 day (τ_{ν}) for large values of viscosity ($\alpha \sim 1$), as observed, but are slow (~ 50 day) for $\alpha \sim 0.01$ (iv) The anti-correlated torque and X-ray luminosity in GX 1+4 is not explained by our model. Also, our model predicts that, in the absence of extraneous perturbations, a star that is spinning up initially eventually transitions to spin down, then evolves toward a state of zero torque, i.e. the model does not exhibit repeated torque reversals in its current, simple form.

The model we have proposed, based on ST93, omits several effects which may be important. First, the disc may generate its own magnetic field via an MHD dynamo, driven by the shear in the mixing layer (as at the solar tachocline). Torkelsson (1998) proposes dynamo action as a mechanism for torque reversals. Second, material may be

transported off the disc to form an outflow or be funnelled onto the stellar poles. For the low magnetic Prandtl numbers adopted in our study ($Pm \approx 10^{-2}$), significant bending of the field lines takes place which might lead to a centrifugal wind (Reyes-Ruiz & Stepinski 1996; Lubow et al. 1994). In the disc outside the mixing layer, the magnetic torque due to such a wind might dominate the viscous torque (Blandford & Payne 1982; Pelletier & Pudritz 1992), whereas our model neglects magnetic torques outside of the mixing layer. Third, the mixing layer may not be thin in the radial direction. For example, even if the magnetic field does not penetrate far into the disc, the KHI may cause the mixing layer to thicken. Fourth, we assume the neutron star to be an aligned rotator, whereas the disc-magnetosphere system behaves differently for an oblique rotator (Wang 1997). Finally, our model does not solve for the disc structure in detail. Ideally, one would combine a detailed solution for the disk structure (e.g. Rappaport et al. 2004) with a detailed model for the location of the inner disk radius (which includes magnetic diffusion among other effects).

ACKNOWLEDGMENTS

This research was funded in part by Australian Research Council Discovery Project grant DP0208735.

REFERENCES

- Aly J. J., 1985, *A&A*, 143, 19
 Aly J. J., 1988, *A&A*, 203, 183
 Baan W. A., 1979, *ApJ*, 227, 987
 Balbus S. A., Hawley J. F., 1991, *ApJ*, 376, 214
 Batchelor G. K., 1953, *The Theory of Homogeneous Turbulence*. Cambridge University Press: London
 Baykal A., Oegelman H., 1993, *A&A*, 267, 119
 Bildsten L., Chakrabarty D., Chiu J., Finger M. H., Koh D. T., Nelson R. W., Prince T. A., Rubin B. C., Scott D. M., Stollberg M., Vaughan B. A., Wilson C. A., Wilson R. B., 1997, *ApJS*, 113, 367
 Blandford R. D., Payne D. G., 1982, *MNRAS*, 199, 883
 Chakrabarty D., Morgan E. H., Muno M. P., Galloway D. K., Wijnands R., van der Klis M., Markwardt C. B., 2003, *Nat*, 424, 42
 Elsner R. F., Lamb F. K., 1977, *ApJ*, 215, 897
 Frank J., King A., Raine D. J., 1992, *Accretion Power in Astrophysics*. Cambridge University Press: London
 Galloway D. K., Chakrabarty D., Morgan E. H., Remillard R. A., 2002, *ApJ*, 576, L137
 Ghosh P., Lamb F. K., 1978, *ApJ*, 223, L83
 Ghosh P., Lamb F. K., 1979a, *ApJ*, 232, 259
 Ghosh P., Lamb F. K., 1979b, *ApJ*, 234, 296
 Ghosh P., Pethick C. J., Lamb F. K., 1977, *ApJ*, 217, 578
 Illarionov A. F., Sunyaev R. A., 1975, *A&A*, 39, 185
 Li J., Wickramasinghe D. T., 1998, *MNRAS*, 300, 1015
 Li L., Narayan R., 2004, *ApJ*, 601, 414
 Liu C. H., Doorly D. J., 2000, *Internat. J. Numer. Methods Fluids*, 32, 29
 Lovelace R. V. E., Romanova M. M., Bisnovatyi-Kogan G. S., 1995, *MNRAS*, 275, 244
 Lubow S. H., Papaloizou J. C. B., Pringle J. E., 1994, *MNRAS*, 267, 235
 Malagoli A., Bodo G., Rosner R., 1996, *ApJ*, 456, 708
 Nelson R. W., Bildsten L., Chakrabarty D., Finger M. H., Koh D. T., Prince T. A., Rubin B. C., Scott D. M., Vaughan B. A., Wilson R. B., 1997, *ApJ*, 488, L117
 Pelletier G., Pudritz R. E., 1992, *ApJ*, 394, 117
 Rappaport S. A., Fregeau J. M., Spruit H., 2004, *ApJ*, 606, 436
 Reyes-Ruiz M., Stepinski T. F., 1996, *ApJ*, 459, 653
 Scharlemann E. T., 1978, *ApJ*, 219, 617
 Shakura N. I., Sunyaev R. A., 1973, *A&A*, 24, 337
 Shapiro S. L., Teukolsky S. A., 1983, *Black Holes, White Dwarfs and Neutron Stars—The Physics of Compact Objects*. John Wiley & Sons
 Spruit H. C., Taam R. E., 1993, *ApJ*, 402, 593
 Torkelsson U., 1998, *MNRAS*, 298, L55
 van der Klis M., 2001, in *AIP Conf. Proc. 599: X-ray Astronomy: Stellar Endpoints, AGN, and the Diffuse X-ray Background Kilohertz quasi-periodic oscillations—observational overview*. pp 406–415
 van Kerkwijk M. H., Chakrabarty D., Pringle J. E., Wijers R. A. M. J., 1998, *ApJ*, 499, L27
 Wang Y.-M., 1987, *A&A*, 183, 257
 Wang Y.-M., 1997, *ApJ*, 475, L135
 Wang Y.-M., Robertson J. A., 1984, *A&A*, 139, 93
 Yi I., Vishniac E. T., 1999, *ApJ*, 516, L87

This paper has been typeset from a *TeX*/ *LT_EX* file prepared by the author.